Establishing structure-function relationship for molecular sieving:

Dissipative particle dynamics simulation of DNA polymers

†*Xiangyang Gao[1], Jian-Sheng Wang[2,3], Gui-Rong Liu[4] , Jongyong Han[5,3]

[1]School of Aeronautics, Northwestern Polytechnical University, Xi'an, P.R. China 7100721.
[2]Department of Physics, National University of Singapore, 2 Science Drive 3, Singapore 117542
[3]Singapore-MIT Alliance, E4-04-10, 9 Engineering Drive 1, Singapore 117576
[4]School of Aerospace Systems, University of Cincinnati, USA.
[5]Department of Biological Engineering, Massachusetts Institute of Technology, Cambridge, MA02139, USA
†*Corresponding and presenting author: xygao@nwpu.edu.cn

Abstract

Detailed modeling of entropic trapping and separation of long DNA molecules in nanofilter array devices is required in order to determine the impact of subtle changes in device structure on the overall separation performance. In this paper, we further developed the previously reported dissipative particle dynamics (DPD) simulation, a modified wormlike chain model is employed to supply a moderate restoring force on particles when they deviate extremely away from their equilibrium positions. Based on this model, we applied our DPD algorithm to two nano-fluidic filters of different geometries. Apart from the general opinion that a longer DNA chain has higher chance to enter the shallow channel, our studies suggested an additional mechanism for the observed length-dependency of DNA mobility. If the coiled length of a short DNA chain is much smaller than half depth of the trap, it is easily hindered in one corner of the trap where the electric field is rather low, which traps the DNA for a longer time. Our studies also showed that the nominal mobility of DNA chains depends on the geometry of the filter. In the two geometries studied, the nano-channel in the center of the trap more efficiently separates long DNA chains. In different geometries, DNA chains experience different folding ratio when it is hindered in the trap, which might lead to different separation rate. Our studies suggested that the recently realized vertical nano-channel membrane systems should exhibit higher DNA selectivity, compared with the previous, planar nanochannel systems.

Keywords: Dissipative particle dynamics (DPD) method, electroosmotic flows, DNA electrophoresis, nano-fluidic filter, wormlike chain model, DNA separation.

Introduction

Separation of proteins and nucleic acids has found increasing applications in studying and sequencing these biological samples [1][2]. Gel electrophoresis has been widely used for separation of DNA by length, but its efficiency deteriorates significantly for longer DNA molecules (>40kpb). Moreover, the study of the sieving mechanism of gel electrophoresis is limited because little information on the structure and pore size of gels are available [3][4]. A variety of micro fabricated micro/nano fliudic systems have been developed to separate DNA molecules [5]-[9]. One important advantage of the microfabricated systems is that their pore sizes can be precisely controlled. Among these micro/nano fluidic systems, Han and coworkers[3][4][8][9] fabricated nanofilter array chips by conventional photolithography and reactive ion etching techniques on a silicon wafer, the nanofilter array chip consists of alternating thin and thick regions in a micro-fabricated channel (T-channel in short). The entropic trapping in the thick region limits the overall mobility of DNA molecules in the channel and the mobility of DNA becomes length-dependent, with longer DNA molecules

have higher mobility in this channel. More recently, Mao and Han[10] developed a novel nanofilter membrane structure with higher throughput than previous planar nanochannels [11].

These different nanochannel geometries of nanofilter / nanomembrane systems would often yield substantially different sieving phenomena, even with the same characteristic nanofilter size. This is because biomolecule sieving in these artificial nanofilter systems is a complicated, multi-scale problem with many different factors involved, such as biopolyelectrolyte conformation and stochastic motion of biomolecules. To explain the experimental findings and facilitate the development of more efficient nanofilters, Monte Carlo simulation [12][13], Brownian dynamics simulations [14][15] and continuum transport model [16], have been used to study the separation process in the nanofilters. In these studies, the solvent flow has not been explicitly modeled and thus the electroosmotic flow (EOF) and hydrodynamic interaction have been neglected. Tessier and Slater [17] have used molecular dynamics (MD) simulation to model the EOF in a narrow filter. In those simulations, the charged particles have been explicitly simulated. This method may provide an accurate result for small systems but becomes less effective for modeling realistic nanofilters because of its high computational cost. Dissipative particle dynamics (DPD) is a mesoscopic simulation method, it has been used in studying various complex systems such as polymer suspensions [18][19], colloids [20][21], multi-phase fluids [22][23], DNA suspension [24]-[26] and recently DNA separation in micro/nano-filter [27][28]. The time and length scale of DPD cover those of realistic micro/nano-fluidic devices, and fluctuating hydrodynamics is considered which is important for DNA separation.

In this paper, we are applying the DPD method to evaluate the difference in nanofilter sieving characteristics due to the subtle differences in nanochannel geometry. Our study is motivated by the development of novel, high-throughput nanofilter membrane structure [10]. While the new vertical nanochannels are ideal for high-throughput molecular processing, careful modeling and characterization of this new structure, compared with planar nanochannels [11] made by “etch-and-bond” method, has not been done. In this work, we further developed the DPD algorithm [27][28] that considers both electroosmotic flow and DNA electrophoresis in nano-fluidic devices and applied the method to determine the sieving characteristics of two different nanofilter designs. Distribution of electric field was calculated with commercial finite element package, *ANSYS*. A modified wormlike chain model is employed to supply a moderate restoring force on particles when they deviate extremely away from their equilibrium positions. The new algorithm balances both stability and efficiency. Our simulation algorithm was tested rigorously to be robust and reliable and was validated against several experimental findings. We used our new DPD algorithm to numerically study the separation of DNA molecules in micro/nano-fluidic filters. Two filters of different geometries were simulated to illustrate the geometry dependence nature of the separation mechanism of DNA chains.

Methodology

DPD algorithms

DPD method has been first introduced by Hoogerbrugge and Koelman [29] for studying the hydrodynamic behavior of complex fluid. This method is based on the simulation of soft spheres, whose motion is governed by certain collision rules. A particle in DPD method is represented as a cluster of molecules rather than a single molecule in the molecular dynamic (MD) simulation. As a result, the length and time scales of a DPD system are much larger than that of MD.

DPD method simulates the motions of ensemble of particles or pseudo particles and each particle is defined by its position, velocity, and mass. The motion of DPD particles is governed by Newton's equations of motion. Interactions between particles are assumed to be pairwise additive, the positions and velocities of DPD particles are calculated as,

$$\frac{d\mathbf{r}_i}{dt} = \mathbf{v}_i, \qquad \text{and} \qquad \frac{d\mathbf{v}_i}{dt} = \sum\nolimits_{j \neq i} \mathbf{f}_{ij} + \mathbf{f}_e \tag{1}$$

Where $\mathbf{r}_i$ and $\mathbf{v}_i$ are the position and velocity vectors respectively of particle *i*. It has been assumed that all particles have identical mass which is normalized to unity. $\mathbf{f}_e$ is the external force. $\mathbf{f}_{ij}$ is the inter-particle force acting on particle *i* by particle *j*, which consists of three parts: conservative force $\mathbf{F}_{ij}^C$, dissipative force $\mathbf{F}_{ij}^D$, and random force $\mathbf{F}_{ij}^R$, i.e.,

$$\mathbf{f}_{ij} = \mathbf{F}_{ij}^C + \mathbf{F}_{ij}^D + \mathbf{F}_{ij}^R \tag{2}$$

The summation of force in Eq. (1) runs over all other particles within a certain cutoff radius, which may vary for different forces. The conservative force is given by

$$\mathbf{F}_{ij}^C = \begin{Bmatrix} a_{ij}(1 - \frac{r_{ij}}{r_c})\hat{\mathbf{r}}_{ij}, & (r_{ij} < r_c) \\ 0, & (r_{ij} \geq r_c) \end{Bmatrix} \tag{3}$$

where a_{ij} is the maximum repulsion between particles *i* and *j*; $\mathbf{r}_{ij} = \mathbf{r}_i - \mathbf{r}_j$, $\hat{\mathbf{r}}_{ij} = \mathbf{r}_{ij} / \left|\mathbf{r}_{ij}\right|$ is the unit vector directed from *j* to *i*. r_c is a cut-off radius. In a complex system, each component is represented by a group of particles. The different values of a_{ij} have to be specified to characterize the interaction of particles in each component or between components. The dissipative force and random force are given by

$$\mathbf{F}_{ij}^D = -\gamma \omega^D(r_{ij})(\hat{\mathbf{r}}_{ij} \cdot \mathbf{v}_{ij})\hat{\mathbf{r}}_{ij} \tag{4}$$

and

$$\mathbf{F}_{ij}^R = \sigma \omega^R(r_{ij})\theta_{ij}\hat{\mathbf{r}}_{ij} \tag{5}$$

where $\mathbf{v}_{ij} = \mathbf{v}_i - \mathbf{v}_j$, γ and σ are two coefficients characterizing the strengths of the dissipative and random forces, ω^D and ω^R are *r*-dependent weight functions which vanishes for $r_{ij} \geq r_c$, and θ_{ij} is white noise function with the following properties,

$$\left\langle \theta_{ij}(t) \right\rangle = 0 \quad \text{and} \quad \left\langle \theta_{ij}(t)\theta_{kl}(t') \right\rangle = (\delta_{ik}\delta_{jl} + \delta_{il}\delta_{jk})\delta(t - t') \tag{6}$$

To satisfy the fluctuation-dissipation theorem , the weight function is required following conditions.

$$\omega^D(r_{ij}) = \omega^R(r_{ij})^2 \qquad \text{and} \qquad \gamma = \frac{\sigma^2}{2k_B T} \tag{7}$$

Where k_B is the Boltzmann constant and *T* the temperature of the system. The weight function is calculated by

$$\omega^D(r_{ij}) = \omega^R(r_{ij})^2 = \begin{Bmatrix} \sqrt{1 - r_{ij}/r_c}, & (r_{ij} < r_c) \\ 0, & (r_{ij} \geq r_c) \end{Bmatrix} \tag{8}$$

EOF theory

EOF is generated due to the Coulombic force acting on counterions and co-ions in an electric double layer (EDL)[30]. The thickness of the EDL is characterized by the Debye length (λ), which is defined by,

$$\lambda = \sqrt{\frac{\varepsilon_0 \varepsilon_b k_B T}{2 N_A C e^2}} \tag{9}$$

Where k_B is the boltzmann constant, T is temperature, ε_0 and ε_b are the permittivity of vacuum and the dielectric constant of fluid respectively, N_A is the Avogadro's number, C is the ionic strength.

The layer of mobile charges moves under the influence of the applied electric field, pulling the liquid within them. The liquid movement is carried through to the rest of the liquid in the channel by viscous force. The calculation of the real EOF field is really a hard work [31], however, when the Debye length is small compared to the characteristic length-scale of a study system, Cummings et al. [32] unveiled that the resulting fluid velocity is proportional to the local electric field, and the constant of proportionality is everywhere the same if the flow is steady and the fluid and electric properties are uniform. The fluid velocities on all wall boundaries satisfy

$$\mathbf{U}_{\text{Wall}} = -\frac{\varepsilon_0 \varepsilon_0 \zeta \mathbf{E}}{\eta} \tag{10}$$

Where $\mathbf{E}$ is the local electric field, η is the fluid viscosity and ζ is the zeta potential which has an approximated relation with ionic strength proposed by [33],

$$\zeta = 0.0288 C^{-0.245} (\text{mV}) \tag{11}$$

Where C represents ionic strength measured in moles/liter.

Worm-like chain model

The mechanical properties of a single DNA molecule have been studied extensively in experiments. Smith et al. [34] conducted a direct mechanical measurement of the elasticity of single DNA molecules by using magnetic beads; Perkins et al. [35] also measured the extension of a tethered DNA molecule in a uniform flow. Based on experiment observations, quite a few models for DNA molecules have been proposed [36]-[39]. It was found that the mechanical properties of DNA molecules in an aqueous solution can be realistically modeled by wormlike chains. The spring force for a chain segment can be expressed as [36]

$$\mathbf{F}_{ij}^{W} = \frac{k_B T}{4P}\left[(1 - \frac{r_{ij}}{l})^{-2} + \frac{4 r_{ij}}{l} - 1 \right] \hat{\mathbf{r}}_{ij} \tag{12}$$

Where $\mathbf{r}_{ij}$ is the distance of bead i and j, l is the maximum length of one chain segment and P is the effective persistence length of the chain. Bustamante et al. [39] found the persistence length for their unlabeled DNA molecules to be 53nm. The typical persistence length in a wormlike model is chosen to be 50nm for modeling standard DNA chains [40].

In Eq. (12), the first term increases to infinity when r_{ij} is close to l, which leads the motion of particles unstable if the time step is not small enough. In addition, if r_{ij} is great than l, the spring force in Eq. (12) decreases drastically, it costs too much a long time for the particle to restore around its equilibrium position. To overcome these shortcomings, Eq. (12) is modified as following,

$$\mathbf{F}_{ij}^{W} = \begin{cases} \dfrac{k_B T}{4P}\left[(1 - \dfrac{r_{ij}}{l})^{-2} + \dfrac{4 r_{ij}}{l} - 1 \right] \hat{\mathbf{r}}_{ij}, & \dfrac{r_{ij}}{l} < \alpha_{\text{lim}} \\ \dfrac{k_B T}{4P}\left[(1 - \alpha_{\text{lim}})^{-2} + 4\alpha_{\text{lim}} - 1 \right] \hat{\mathbf{r}}_{ij}, & \dfrac{r_{ij}}{l} \geq \alpha_{\text{lim}} \end{cases} \tag{13}$$

A constant ratio between r_{ij} and l, α_{lim}, is introduced. If r_{ij}/l is great than α_{lim}, a moderate force applied on the particles to accelerate the process of restoring to their equilibrium positions. The force should be big enough to let polymer particles restoring quickly, but too big a force requires a small enough time step which makes the simulation unaffordable. After balancing the restoring process and the efficiency of simulation, in our simulation, α_{lim} is set to 0.98, the maximum restoring force is about 20 times of the maximum conservative force.

DNA Electrophoresis

Electrophoresis refers to the motion of charged particles in a stationary liquid phase [30]. When an electric field is applied, the charged particle will move in the liquid towards either the cathode or the anode depending on the sign of the surface charge of the particle. DNA molecules are usually charged under an electric field. In DNA electrophoresis, electrostatic interactions and the resulting fluid shearing mainly occur within the Debye layer, which under the conditions here is very thin. As a result of these screening processes, the DNA electrophoretic mobility becomes independent of the strand contour length. Accurate modeling of this phenomenon requires explicit modeling of counter-ion charges, which is difficult and prohibitively expensive. To avoid this limitation, Duong-Hong et al. [28] proposed a simple treatment for the interaction between DNA and solvent particles in free draining situations. It assumed that when the distance between a fluid particle and a DNA particle becomes smaller than the Debye length, the fluid particle acquires a counter-charge, i.e., a positive charge equal to the value of the DNA-bead charge. The fluid particle is then subject to an electric force that is equal to the one exerted on DNA particles, but in the opposite direction. The electric force for a particle with charge q is given by

$$\mathbf{f}_{\text{EP}} = q\mathbf{E} \tag{14}$$

Simulation procedures and parameters

We first computed the electric field in the computational domain. This can be done by directly solving the Laplace equation subject to von Neumann boundary condition at the walls with differential method. For a better accuracy, we get the distribution of electric field with commercial finite element package, *ANSYS*. With the distribution of electric field, we can compute the electrostatic velocity at the wall, U_{wall}, (in reality a Debye length away from the wall) by using Eq. (10) and the given zeta potential in Eq. (11).

The velocity, U_{wall}, is locally assigned to the wall particles; the ‘‘moving wall’’ then drags the fluid particles by viscosity. In DPD, due to the ‘soft’ repulsive force, particles sometimes may penetrate the wall and exit the computational domain. To prevent this motion we apply a double layer wall structure [41], as well as a bounce-back boundary condition [42] for particles which penetrate the wall. This condition serves as a no-slip boundary condition and resetting the positions and velocities of particles exiting the domain to the new ones. Periodic boundary conditions are applied to the flow domain to reserve the mass continuity.

To update the electric force on DNA particles and solvent particles in the vicinity of a DNA particle using Eq. (14), we input the computed distribution of electric field by discretising the simulation domain into small cells. Each cell has a representative vector of electric field. The equations of motion (Eq. 1) are sloved by using the velocity-Verlet algorithm suggested by Groot and Warren [26]. At every time step, the set of positions and velocities, $\{\mathbf{r}_i, \mathbf{v}_i\}$ are updated from the positions and velocities at earlier time step using the following scheme:

$$\mathbf{r}_i(t+\delta t) = \mathbf{r}_i(t) + \delta t\mathbf{v}_i(t) + \tfrac{1}{2}\delta t^2\mathbf{f}_i(t) \tag{15}$$

$$\tilde{\mathbf{v}}_i(t+\beta\delta t) = \tilde{\mathbf{v}}_i(t) + \beta\delta t\mathbf{f}_i(t) \tag{16}$$

$$\mathbf{f}_i(t+\delta t) = f(\mathbf{r}_i(t+\delta t), \tilde{\mathbf{v}}_i(t+\beta\delta t)) \quad (17)$$

$$\mathbf{v}_i(t+\delta t) = \mathbf{v}_i(t) + \tfrac{1}{2}\delta t(\mathbf{f}_i(t) + \mathbf{f}_i(t+\delta t)) \quad (18)$$

The DPD parameters of repulsive coefficient are calculated based on the previous works of [25][26]. We use β=0.5 in the above Verlet-type algorithm, and the coefficient of random force between fluid particles σ=3, with these parameters, the time step δt can be up to 0.06. The density of solvent is chosen to be 0.1, and the cut off radius r_c is set to 2.0. Repulsive coefficient between fluid particles is set as 375 to maintain a similar compressibility of water (about 16).

Non-dimensional parameters are constructed by using the length unit [σ]=18nm, the mass unit [m]=2×10^{-14} kg and energy unit [ε]=k_BT=4.14×10^{-21} J, the time unit [t] is then calculated as $\sqrt{m\sigma^2/\varepsilon}$ ~ 39.5μs. The time step, δt, is chosen as 0.01[t]. We choose the maximum segment length of DNA chain to be 2.55[σ].

Assuming that the electrical charge is uniformly distributed along each DNA segment, the effective charge of a DNA segment is suggested to be 0.02e[28]. As stated in the previous section, to capture the free draining mobility, the fluid particles should be allowed to access chain particles, the coefficient of repulsion between fluid and chain particles is chosen as 1 to maintain a low interaction. The random force between fluid and chain particles is adjusted from the free draining mobility in experiment, from the model validation in the next section, it is chosen as 0.5 in our simulation.

Results and discussions

Model validation

To validate our simulation model, the free draining mobility (μ_0) of various DNA chains was computed over an electrical field range of 20-120V/cm at 10mM TBE, the ionic concentration is similar to the experiment of Nkodo et al [40]. Mobility is calculated as gradient of velocity against electric field. The density and the viscosity of solvent are 1000kg/m^3 and 8.9×10^{-4} Pa.s, respectively. 5 DNA chains corresponding to 3 molecular weights of DNAs are suspended in water particles. The molecular weight and number of DNA chains are listed in table 1. DNA chains and water particles are placed in a large straight channel which is confined in the *z* direction (height of channel) and periodic boundary conditions are applied in both *x* and *y* directions (in-plane). The result for different DNA chains are shown in figure 1. μ_0 appears to be independent of DNA molecular weight and in good agreement with experiment results.

Table 1. Molecular weight and number of DNA chains

Molecular weight of DNA (kbp)	107.40	32.26	10.74
Number of chains	1	2	2

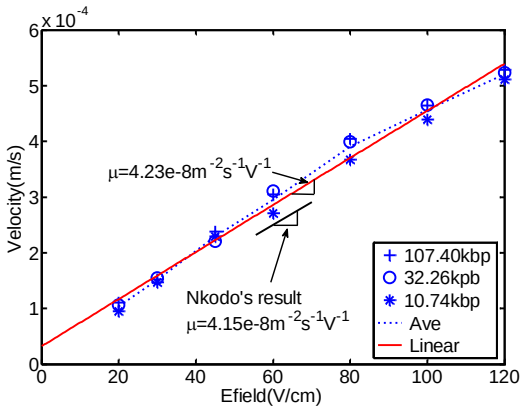

Figure 1. Free-draining mobilities of DNA chains

The simulation was then applied to nano-filters proposed by Han and Craighead [9]. The ionic concentration is 5×TBE, the effective charge per base pair was suggested as 0.012e [28] because the mobility decreases by approximately 10% when ionic strength doubles [43]. Compared with the free draining mobility in the large straight channel, the nominal mobilities of DNA chains in the nano-filter are rather low, this leads to an extreme long simulation time which is required before we can get a reliable result. To save the simulation time, we can reduce the coefficient of random force, σ, between the DNA particle and the fluid particle from 0.5 to 0.2.

The simulation is first carried out without the electric forces and the electroosmotic flow. The temperature and pressure become stable after 300~1000[t]. Then the electroosmotic flow and the electric forces are applied. A longer time of simulation will be carried out thereafter, about 10^4~10^5 [t].

Simulation results

Two geometries as shown in figure 2 are selected in simulation to study the geometry dependence of separation capability. The first geometry is similar as a characteristic cell of the nano-filter in Han's experiment [9], the thin channel is located at the upper end of the trap. And in the second geometry, the thin channel is located at the center of the trap. In both geometries, length of cell (x-axis) is 200[σ], the channel and the trap have equal length; in z-axis, the thickness of the nano-channel is 5[σ], and the height of the trap is 50[σ]; in y-axis, the depth is 80[σ]. Periodic boundary conditions are applied in x- and y- directions. In both geometries, 5 DNA chains are suspended in water particles corresponding to 3 molecular weights of DNAs which is listed in table 1.

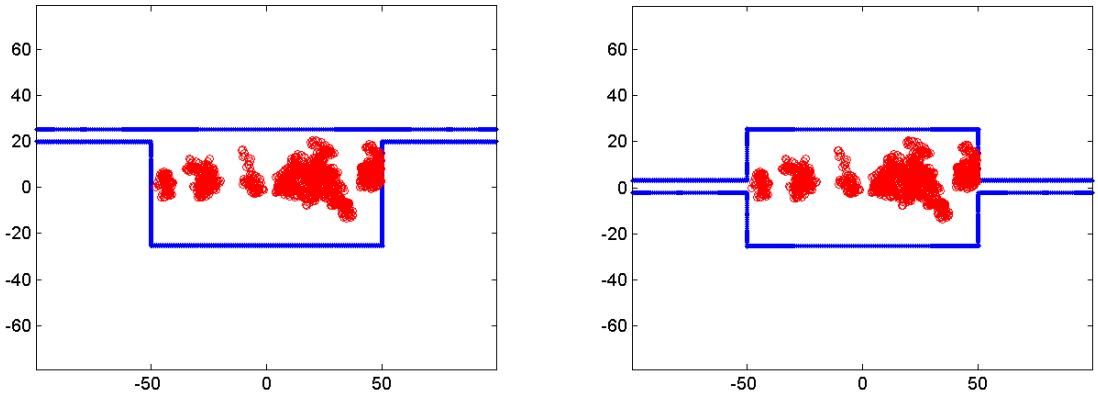

(a) (b)

Figure 2. Geometry projections of the simulated nano-filters in *x*-*z* plane. (a) geometry A, (b) geometry B. (water particles are not shown)

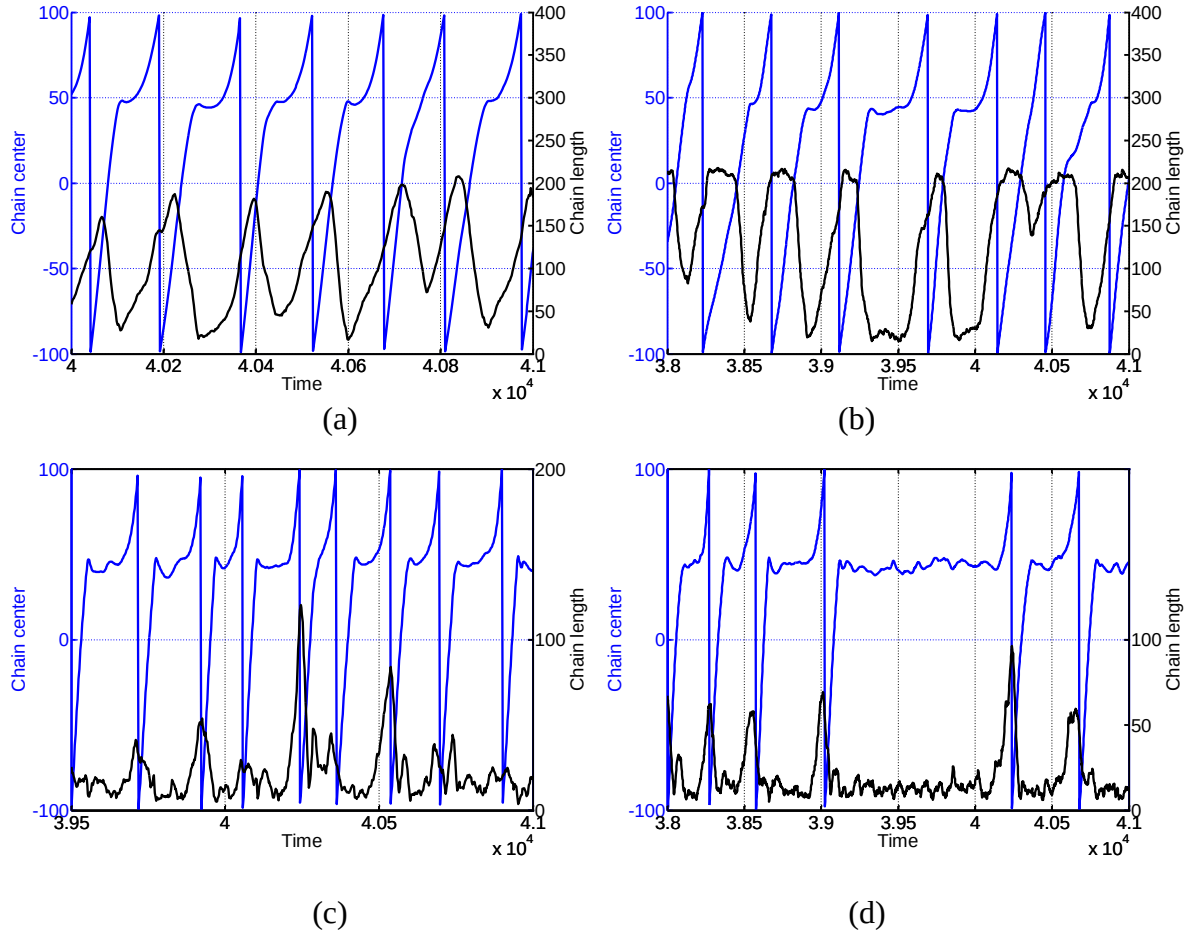

Figure 3. Variation of chain center and chain length in geometry A. (a) 107.4kbp DNA at *E*=100V/cm (b) 107.4kbp DNA at *E*=50V/cm (c) 10.7kbp DNA at *E*=100V/cm (d) 10.7kbp DNA at *E*=50V/cm.

Figure 3 illustrates typical variations of the center position and chain length. Result of the chains of 107.4kbp and 10.7kbp with electrical field 100V/cm and 50V/cm are shown. The motion of DNA chains is alternatively jerky and tethered; correspondingly, the chain was alternatively stretched and coiled. It is clear that the chain is stretched and moves fast at the thin part and is coiled and slows down till to be hindered before the entrance of the thin part. This is similar as the video images observed in experiment [9]. At the same electrical field, the travel time over one period of short chain is much higher than the long chain. The travel time over each period is then evaluated. We simulated for electrical field from 30V/cm to 120V/cm. the travel time in each period is showed in figure 4(a). With the average travel time, the nominal mobility μ, is obtained by the following equation and is illustrated in figure 4(b).

$$\mu = \frac{l}{\tau E} \tag{19}$$

Where l is the length of the simulation region, τ is the average travel time over one period.

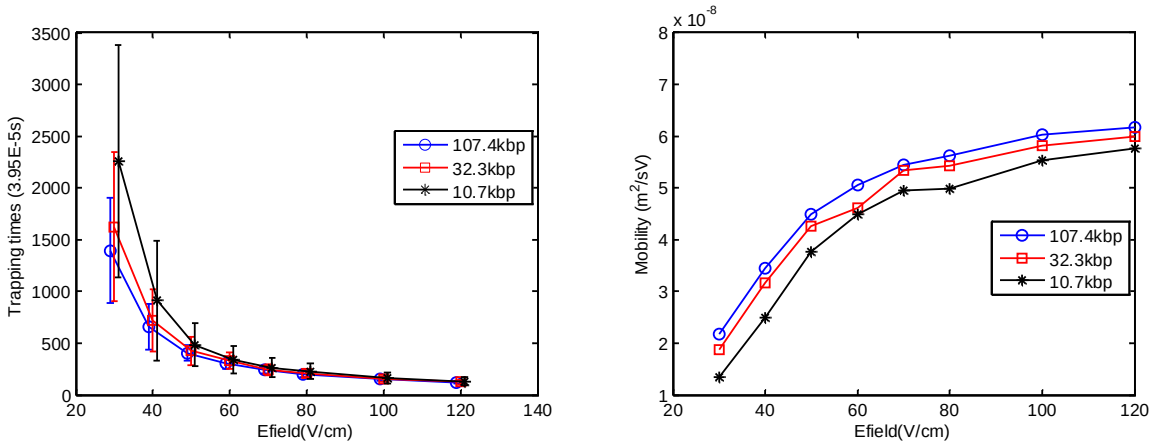

(a) (b)

Figure 4. Travel time in a period (a) and nominal mobility (b) of DNA chains in geometry A.

From figure 4, we can see clearly that the nominal mobility increases with the weights of DNA molecules. Longer DNA chains move faster than the short ones, which is consistent with observations in Han's experiment [9]. The mobilities of all DNA chains tend to converge to a so called "free-draining mobility" at high electric field. To illustrate more clearly the separation capacity of the nano-filter, mobilities of all chains are normalized against the longest chain as mobility ratios which are shown in figure 5.

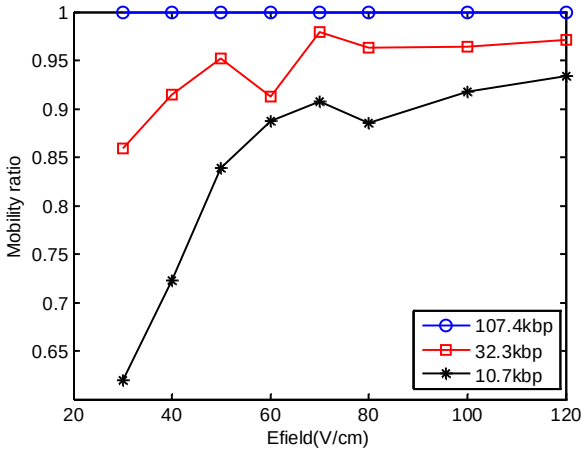

Figure 5. Mobility ratio of DNA chains against the longest chain in geometry A.

Mobility ratio reflects the mobility difference, from figure 5, we can see clearly that the mobility difference decreases with the electric field and tend to be vanished at high electric field. This is consistent with observations in experiment [3][4][8][9] where the size dependence of electrophoretic mobility disappeared when the field was increased.

The travel time over one period and the nominal mobility of DNA in geometry B are shown in figure 6 and the mobility ratio is shown in figure 7.

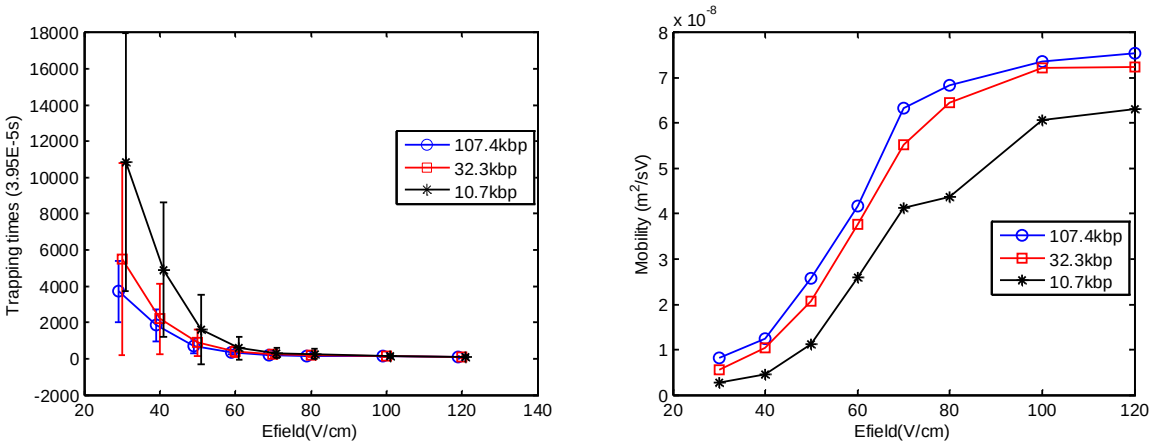

(a) (b)

Figure 6. Travel time in a period (a) and nominal mobility (b) of DNA chains in geometry B.

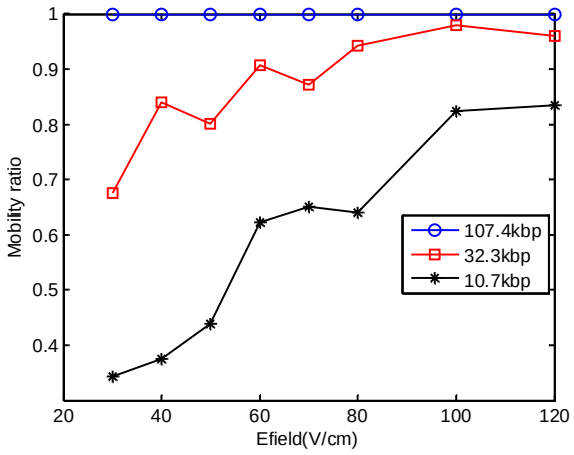

Figure 7. Mobility ratio of DNA chains against the longest chain in geometry B.

The variation of the travel time over one period and the mobility of DNA chains in geometry B are similar with the result in geometry A. But comparing figure 5 with figure 7, we may conclude that the differences of the nominal mobility of DNA chains in geometry B is more significant than that in geometry A. At low electric field, the nominal mobilities of DNA chains in geometry B are less than that in geometry A, however, at high electric field, the nominal mobilities of DNA chains in geometry B are great than in geometry A. In another words, nominal mobilities of DNA chains in geometry B are more sensitive with the electric field.

From figure 3, we know that the length of a DNA chain varies periodically. The length when it is stretched is far great than when it is hindered. So it is interesting to study the length of DNA under these two distinguished states separately. For the stretched state, we evaluate the peak length in each period. For the hindered state, we average the length during the DNA chain is confined in the trap. The length of a DNA chain is represented by the folding ratio which is defined by the ratio between the length of the DNA chain in x-direction and its contour length. Folding ratio at 1.0 refers to fully stretched of a DNA molecule.

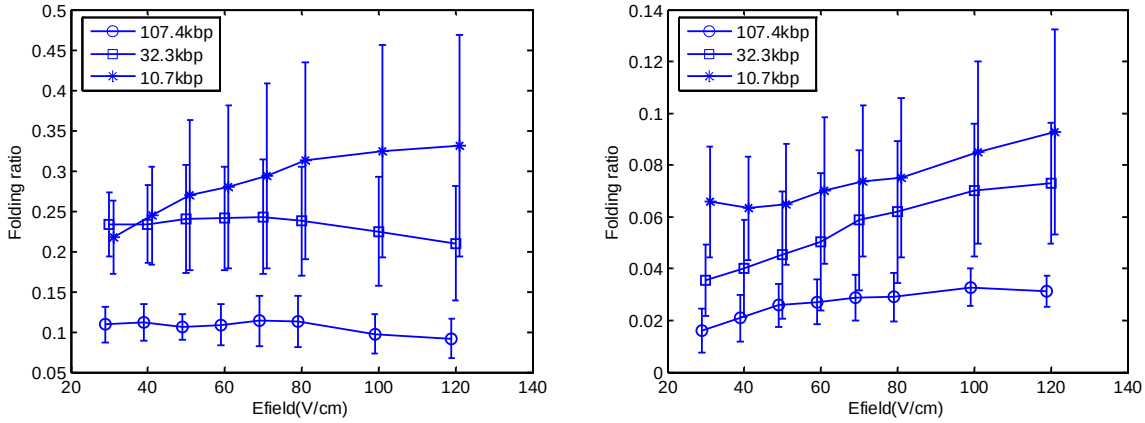

Figure 8. Folding ratio of DNA chains when stretched (a) or hindered (b) in geometry A

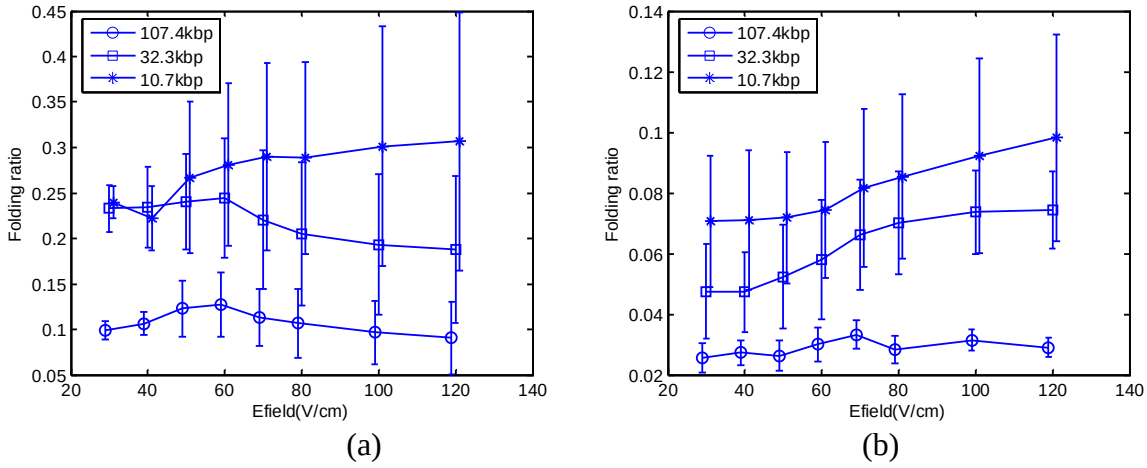

Figure 9. Folding ratio of DNA chains when stretched (a) or hindered (b) in geometry B

Figure 8 shows the folding ratio of DNA chains when stretched and when hindered separately in geometry A. At a stretched state, the folding ratios of two longer DNA chains almost remain the same or slightly lower down with the electric field, while the folding ratio of the shortest DNA chain increases with the electric field. At a hindered state, the average folding ratios of all DNA chains increase with the electric field. It indicates that at high electric field DNA chains are more difficult to be coiled than at low electric field. At both states, folding ratios of DNA chains decrease with the weight of DNAs.

Figure 9 illustrates the folding ratios of DNA chains in geometry B. It is interesting to see that at stretched state the folding ratios of all DNA chains in geometry B are nearly the same as the corresponding result in geometry A. It is reasonable since the length and the thickness of the thin channel in both geometries are same, and thus the local electric field is nearly the same. At hindered state, however, the folding ratios of the DNA chains in two geometries show diversity behaviors depending on their weights. Folding ratios of the shortest DNA chain in geometry A is obviously less than that in geometry B regardless the electric field applied. However, folding ratios of DNA chains of the other two longer chains in two geometries have significant different depending on the applied electric field. At low electric field, the folding ratios of two longer chains in geometry A are obviously lower than that in geometry B. But at high electric field, the folding ratios of two longer chains in two geometries are nearly the same correspondingly.

The geometry dependency of DNA chains is caused by the distribution of electric field and the length of DNA chains. Figure 10 illustrates the contour of magnitude of electric field in both geometries. We only need to analyze DNA chains in hindered state, i.e., in traps.

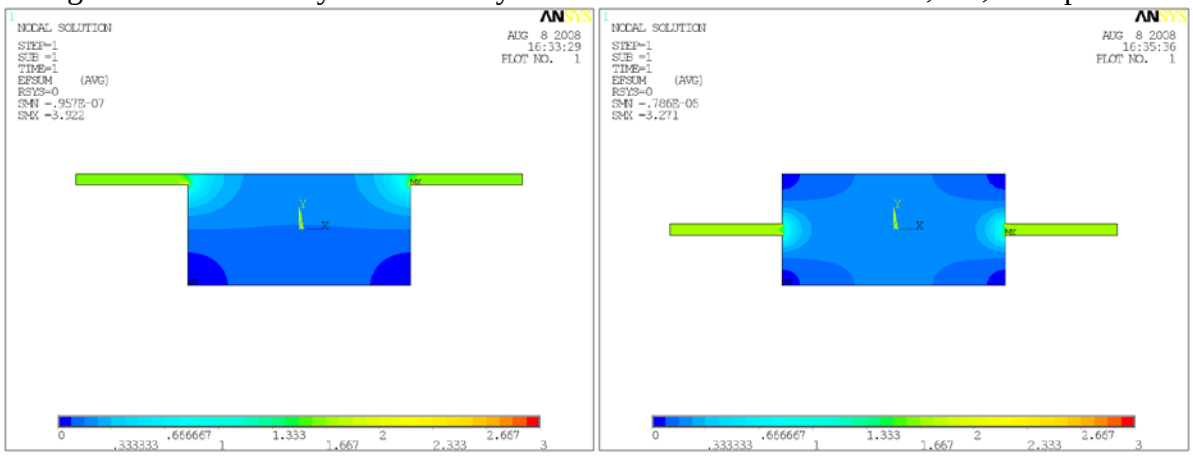

(a) (b)

Figure 10. Contour of the magnitude of electric field in (a) geometry A and in (b) geometry B.

For the two longer chains, the lengths are always longer than half depth of the trap even at low electric field. At low electric field, because the electric force is relative weak, DNA chains are more likely to pass low field regions, i.e., near the bottom corners of the trap. As the depth of the trap in geometry A is about two times of that in geometry B, the segment of a DNA chain within low field regions in geometry A is usually larger than that in geometry B. And because the segment of a DNA chain in low field regions tends to be coiled, the folding ratios of these DNA chains in geometry A are smaller than that in geometry B. At high electric field, since DNA chains are rather long, there is always a big enough segment of DNA chain in each geometry posing high electric field region and thus is subjected a relative strong electric force. This strong electric force is dominant and thus offset the effect of coiling of the rest segment under low electric field region. As a result, folding ratio of these DNA chains in two geometries are almost the same.

For the shortest DNA chain, even the length at high electric field is smaller than half depth of the trap, as a result, DNA chains can still move to low electric field regions, the strong electric force only applied when DNA chains pass the high electric field region. As a result, folding ratio of the shortest DNA chain in geometry A is lower than that in geometry B regardless the applied electric field.

In both geometries, for a long chain, there is hardly a chance the whole coiled chain is located in low electric field region. But for a short chain, because the coiled size is much less there is always a chance moving to the corner of the trap where the electric field is rather small and would probably stay a longer time before it is pushed to the high field region. This is probably another reason of the experiment observation that longer DNA chains have a higher mobility. As the coiled size of the shortest chain is always less than the half depth of the traps (28% at 30V/cm ~40% at 120V/cm), in geometry B, it has double chance to be hindered for a while in low electric field regions. That is why the separation effect is much significant in geometry B than in geometry A.

To illustrate the above analysis, figure 11 plots the trajectories of the DNA mass center in 5 consecutive passes for the simulated three chains. 5 consecutive passes are employed to show

the repeatability as the stochastic effect was included in simulation. The shortest chain tends to pass the low electric field zone (bottom) and thus has a lower mobility, and in geometry B it can move to both the top zone and the bottom zone. In addition, at low electric field the short chains can go further to the low electric field zone and thus has a more significant sieving effect.

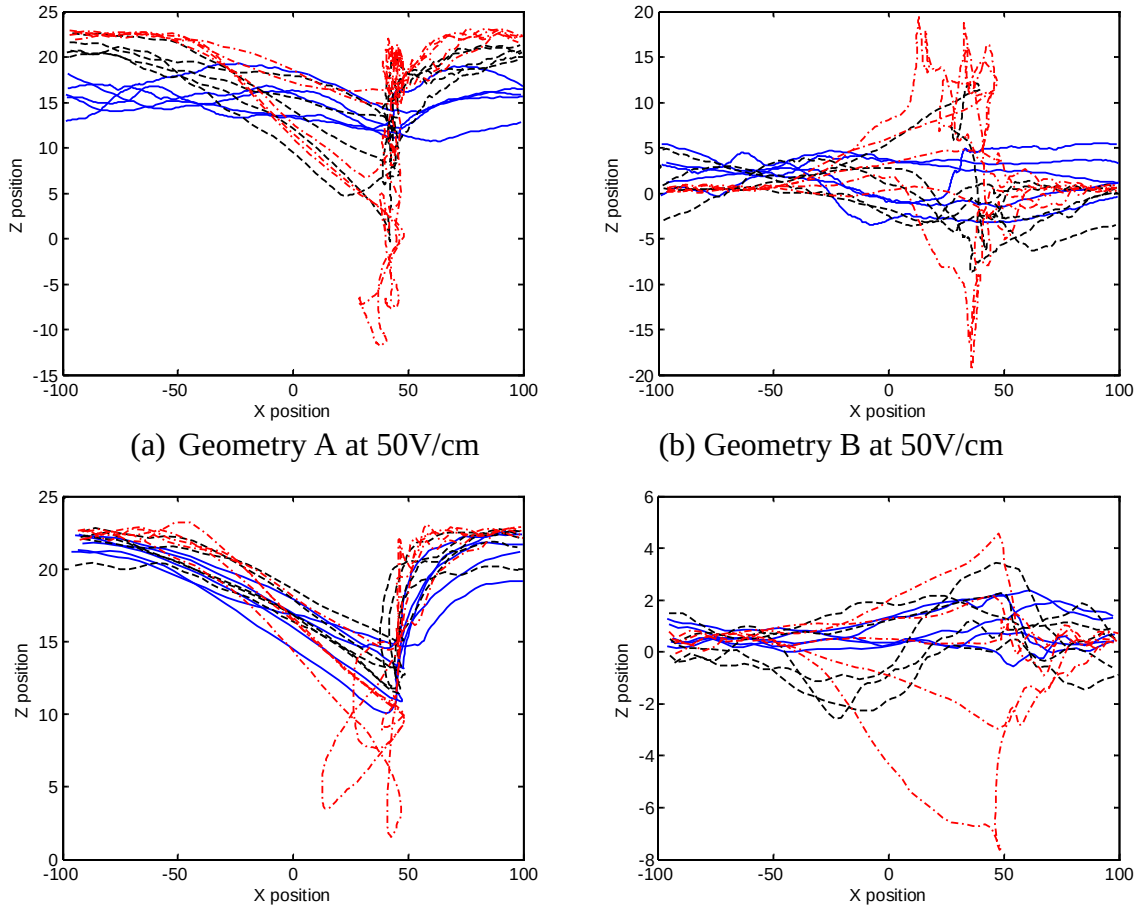

(a) Geometry A at 50V/cm (b) Geometry B at 50V/cm

(c) Geometry A at 100V/cm (d) Geometry B at 100V/cm

Figure 11. Trajectory of mass center of DNA chains. Blue solid line for 107.4kbp, dark dashed line for 32.3kbp and red dash-dotted line for 10.7kbp

General speaking, DNA chains experience different folding ratios when it is hindered in the trap in different geometries. From the above discussion, this might be the reason of the different separation effect in different geometries. This result suggests that we can design and optimize the nano-filter devices for separating a specific mixture of DNA chains.

Conclusions

We further developed a new DPD algorithm considering both DNA electrophoresis and electroosmotic flows in patterned nano-filters. A modified worm-like chain model enables the algorithm robust and efficiency. The nominal mobility of DNA chains was found to increase with their molecular weight which is consistent with the experiment observation. Apart from the general opinion that a longer DNA chain has higher chance to enter the shallow channel, after analyzing the folding ratio of DNA chains in stretched state and in coiled state respectively, our studies suggested an additional mechanism for the observed molecular weight-dependency of DNA mobility. If the coiled length of a short DNA chain is much

smaller than the depth of the trap, it is easily hindered in one corner of the trap where the electric field is rather low, which traps the DNA for a longer time.

The result also shows that the nominal mobility as well as the folding ratio of DNA chains depends on the geometry of nano-filter. Our studies suggested that it is possible to design the geometry of nano-filter devices for optimally separating a specific mixture of DNA chain suspension. Although the results of only two geometries of nano-filter are presented in this paper, our DPD algorithm and model is able to simulate nano-filters with more complex geometries, which will be one of our future works. In addition, the electroosmotic flow in our model is currently confined with small Debye length, if the thickness of the Debye layer is comparable to the thickness of the nanofilter, the shear flow within the Debye layer should also be properly considered, which is another problem need to be solved in the future.

Acknowledgments This work was funded by Singapore-MIT Alliance through the Computational Engineering program.

References

[1] Woods LA, TP Roddy, AG Ewing (2004) Capillary electrophoresis of single mammalian cells. Electrophoresis 25: 1181-7
[2] Marko-Varga G, J Nilsson, T Laurell (2003) New directions of miniaturization within the proteomics research area. Electrophoresis 24: 3521-32
[3] Fu J, Schoch RR, Stevens AL, Tannenbaum SR, Han J (2007) Patterned anisotropic nanofluidic sieving structure for continuous- flow separation of DNA and protein. Nat Nanotechnol 2:121–128
[4] Fu J, Mao P, Han J (2005) A nanofilter array chip for fast gel-free biomolecule separation. Appl Phys Lett 87(1–3):263902
[5] Volkmuth WD and RH Austin (1992) DNA electrophoresis in microlithographic arrays. Nature 358(6387): 600-2,
[6] Volkmuth WD, Duke T, Wu MC, Austin RH and Szabo A (1994) DNA electrodiffusion in a 2D array of posts. Phys, Rev. Lett. 72: 2117-20,
[7] Chou CF, Bakajin O, Turner SWP, Duke TAJ, Chan SS, Cox EC, Craighead HG and Austin RH (1999) Sorting by Diffusion: An Asymmetric Obstacle Course for Continuous Molecular Separation. Proc Nat Acad Sci 96(24): 13762-5
[8] Han J, Turner HG (1999) Entropic Trapping and Escape of Long DNA Molecules at Submicron Size Constriction. Phys. Rev. Lett. 83: 1688-91
[9] Han J, Craighead HG (2000) Separation of long DNA Molecules in a microfabricated entropic trap array. Science 288:1026–1029
[10] Mao P and J Han (2009) Massively-Parallel Ultra-High-Aspect-Ratio Nanochannels as Mesoporous Membranes. Lab on a Chip 9: 586 – 591. DOI: 10.1039/b809370a
[11] Mao P, Han J (2005a) Fabrication and characterization of 20 nm nanofluidic channels by glass-glass and glass-silicon bonding. Lab on a Chip 5: 837 - 844
[12] Tessier F, Labrie J, Slater GW (2002) Electrophoretic separation of long polyelectrolytes in submolecular-size constriction: a Monte Carlo study. Macromolecules 35:4791–4899
[13] Chen Z, Escobedo FA (2003) Simulation of Chain-length Partitioning in a Microfabricated Channel via Entropic Trapping. Mol. Sim. 29: 417-25
[14] Streek M, Schimid F, Duong TT, Ros A (2004) Mechanisms of DNA separation in entropic trap arrays: a Brownian dynamics simulation. J Biotech 112:79–89
[15] Panwar AS, Kumar S (2006) Time scales in polymer electrophoresis through narrow constrictions: A brownian dynamics study. Macromolecules 39(33): 1279-89
[16] ZR Li, GR Liu, YZ chen, J-S Wang, H Bow, Y Chen, J Han (2008) Continuum transport model of Ogstom sieving in patterned nanofilter arrays for separation of rod-like biomolecules. Electrophoresis 29: 329-339
[17] Tessier F, Slater GW (2005) Control and quenching of electroosmotic flow with end-grafted polymer chains. Macromolecules 38:6752–6754
[18] Kong Y, Manke CW, Madden WG, Schlijper AG (1997) Effect of solvent quality on the conformation oand relaxation of polymer via dissipative particle dynamics. J. Chem.. Phys. 107(2): 592-602
[19] Schlijper AG, Manke CW, Madden WG, Kong Y (1997) Computer simulation of non-Newtonian fluid rheology. Int. J. Mod. Phys. C 8(4):919–929

[20] Boek ES, Coveney PV, Lekkerkerken HNW, van der Schoot (1997) Simulating the rheology of dense colloidal suspensions using dissipative particle dynamics. Phys. Rev. E 55(3B):3124– 3133
[21] Koelman JMVA, Hoogerbrugge PJ (1993) Dynamic simulation of hard sphere suspensions under steady shear. Europhys. Lett 21(3):363–368
[22] Coveney PV, Novik KE (1996) Computer simulations of domain growth and phase separation in 2D binary fluids using dissipative particle dynamics. Phys. Rev. E 54(5):5134–5141
[23] Coveney PV, Espanol P (1997) Dissipative particle dynamics for interacting multi-component systems. J. Phys. A. Maths Gen. 30(3):779–784
[24] Fan XJ, N Phan-Thien, TY Ng, XH Wu and D Xu (2003) Microchannel flow of a macromolecular suspension. Phys. Fluids 15:11
[25] Fan XJ, N Phan-Thien, S Chen, XH Wu, TY Ng (2006) simulating flow of DNA suspension using dissipative particle dynamics. Physics of Fluids 18: 063102,
[26] Groot RD, Warren PB (1997) Dissipative particle dynamics: bridging the gap between atomic and mesoscopic simulation. J. Chem. Phys. 107(11):4423–4435
[27] Duong-Hong D, J-S Wang, GR Liu, YZ Chen, J Han, NG Hadjiconstantinou (2008a) Dissipative particle dynamics simulations of electroosmotic flow in nano-fluidic devices. Microfluidics and Nanofluidics 4:219
[28] Duong-Hong D, J Han, J-S Wang, NG Hadjiconstantinou, YZ Chen, and GR Liu (2008b) Realistic simulations of combined DNA electrophoretic and electroosmotic flows in nano-fluidic devices. Electrophoresis 29: 4880
[29] Hoogerbrugge PJ, Koelman JMVA (1992) Simulating microscopic hydrodynamic phenomena with dissipative particle dynamics. Europhys. Lett. 19(3):155–160
[30] Li DL (2004) Electrokinetics in microfluidics pp92-130. Elsevier academic press.
[31] Patankar NA, Hu HH (1998) Numerical simulation of electroosmotic flow. Anal Chem 70:1870–1881
[32] Cummings EB, Griffiths SK, Nilson RH, Paul PH (2000) Conditions for similitude between the fluid velocity and electric field in electroosmotic flow. Anal Chem 72:2526–2532
[33] Pennathur S and Santiago JG (2005) Electrokinetic transport in nanochannels. 2. Experiments. Anal Chem 77:6782–6789
[34] Smith SB, L Finzi, and C Bustamante (1992) Direct mechanical measurements of the elasticity of single DNA molecules. Science 258: 1122.
[35] Perkins TT, DE Smith, RG Larson and S Chu (1995) Stretching of a single tethered polymer in a uniform flow. Science 268: 83
[36] Shaqfeh ESG (2005) The dynamics of single-molecule DNA in flow. J N-N Fluid Mech 130:1–28
[37] Larson RG, TT Perkins, DE Smith, and S Chu (1999) The hydrodynamics of a DNA molecule in a flow field. Flexible Polymer Chain Dynamics in Elongational Flow, Theory and Experiments, edited by TQ Nguyen and HH Kausch, Springer, New York, pp. 259–282
[38] Vologodskii A (1994) DNA extension under the action of an external force. Macromolecules 27: 5623
[39] Bustamante C, JF Marko, ED Siggia and S Smith (1994) Entropic elasticity of -phage DNA. Science 265: 1599
[40] Nkodo AE, Garnier JM, Tinland B, Ren H, Desruisseaux C, McCormick LC, Drouin G, Slater GW (2001) Diffusion coefficient of DNA molecules during free solution electrophoresis. Electrophoresis 22:2424–2432
[41] Duong-Hong D, Phan-Thien N, Fan XJ (2004) An implementation of no-slip boundary conditions in DPD. Comput Mech 35:24–29
[42] Willemsen SM, Hoefsloot HCJ, Iedema PD (2000) No-slip boundary condition in dissipative particle dynamics. Int J Mod Phys C 11(5):881–890
[43] Long D, JL Viovy, A Ajdari (1996) Stretching DNA with electrical fields revisited. Biopolymers 39: 755

Biography

Dr Gao Xiangyang obtained his PhD from Northwestern Polytechnical University and Nanyang Technical University, and was a Research Fellow in Nanyang Technical University and National University of Singapore. He has been an Associate Professor in School of Aeronautics, Northwestern Polytechnical University, P.R. China since 2010. His research interests include modeling of shape memory materials and particle simulation methods in various applications.